JOURNAL OF SPACECRAFT AND ROCKETS
Vol. 44, No. 5, September–October 2007

Initial Sizing and Reentry-Trajectory Design Methodologies for Dual-Mode-Propulsion Reusable Aerospace Vehicles

Vicent Garcia Tormo* and Varnavas C. Serghides†
Imperial College London, London, SW7 2AZ England, United Kingdom

DOI: 10.2514/1.30613

An evaluation of the current state of the commercial space sector in conjunction with the ever-increasing presence of micro- and minisatellites in the telecommunication market stresses the requirement to establish an economically feasible launch capability for relatively small satellites. The aim of this paper is to present a series of design methodologies that will enable the initial design of dual-propulsion uninhabited aerospace vehicles with horizontal-takeoff-and-landing capabilities, which will fill this niche in the space launch sector. A concept-specific initial sizing methodology is presented with a trajectory design tool that integrates aerodynamic heating with descent trajectory optimization, which together form part of the development of a complete design methodology embedded in a visually interfaced software program.

Nomenclature

A, B	=	generic regression-line constants
$A_{\max}$	=	maximum cross-sectional area
$C_{Dl\&p}$	=	leakage and protuberances drag coefficient
$C_{D\text{misc}}$	=	miscellaneous drag coefficient
C_{Do}	=	parasite drag coefficient
$C_{D\text{wave}}$	=	wave drag coefficient
C_f	=	skin friction coefficient
$C_{L\text{design}}$	=	design lift coefficient
C_P	=	specific heat coefficient
D	=	drag force
E_{WD}	=	empirical wave-drag-efficiency factor
FF	=	form factor
f, f'	=	generic function
g	=	gravitational acceleration
H	=	enthalpy
h	=	altitude
h_e	=	energy height
I_{SP}	=	specific impulse
J	=	mechanical equivalent of heat
K_1, K_2	=	stagnation heating factors
L	=	lift force
LF_{DD}	=	drag-divergent lift-adjustment factor
l	=	fuselage length with nonconstant cross-sectional area
M	=	Mach number
M_{CR}	=	critical Mach number
M_{DD}	=	drag-divergent Mach number
$M_{\text{DD}\,L=0}$	=	zero-lift drag-divergent Mach number
M_{final}	=	fuel mass at orbit
M_{initial}	=	fuel mass at rocket ignition
m	=	vehicle mass
$\dot{m}$	=	propellant mass burn rate
P_s	=	specific excess power
p	=	pressure
Q	=	interference factor
q	=	heat rate
R	=	Earth's radius
r	=	body radius
f_s	=	change in specific energy per change in fuel weight
S	=	solar and nocturnal heat radiation
S_{ref}	=	reference area
S_{wet}	=	wetted area
T	=	thrust force
$T_{\max}$	=	rocket-engine maximum thrust
T_{surf}	=	transient surface temperature
T_w	=	surface temperature
T/W	=	thrust-to-weight ratio
t	=	time
V	=	velocity
W_e	=	vehicle empty weight
W_{fuel}	=	fuel weight
W_{payload}	=	payload weight
$W_{\text{propellant}}$	=	propellant weight
W_{rocket}	=	rocket-engine weight
W/S	=	wing loading
W_x/W_0	=	mission weight fraction
W_0	=	design takeoff weight
z	=	air-compressibility factor
α	=	angle of attack
β	=	radiation coefficient
δ	=	rocket thrust angle
γ	=	flight path angle
Δt	=	change in time
ΔV	=	change in velocity
Λ	=	sweep angle
μ	=	viscosity
ρ	=	density
τ	=	material thickness
ϕ	=	bank angle
χ	=	heading angle

Subscripts

c	=	component
LE	=	leading edge
LND	=	landing
max	=	maximum
R	=	recovery
TO	=	takeoff
st	=	stagnation
w	=	wall
∞	=	freestream conditions

Presented as Paper 7292 at Space 2006, San Jose, CA, 19–21 September 2006; received 23 February 2007; revision received 27 April 2007; accepted for publication 27 April 2007.

*Research Student, Department of Aeronautics, South Kensington Campus. Student Member AIAA.

†Senior Lecturer, Department of Aeronautics, South Kensington Campus. Senior Member AIAA.

I. Introduction

THE commercial exploitation of the satellite market is heavily dependent on launch costs. The currently available launch methods are expensive and therefore limit the use of space to heavy-communication-satellite deployment or bulk transport to low Earth orbit.

Apart from the Space Shuttle *Orbiter*, all current launch vehicles are expendable. A key factor in the design of future space transportation systems is reusability. However, since the first space shuttle flight more than 20 years ago, the aerospace sector has not seen any major developments regarding vehicle reusability. Furthermore, the development of a more cost-effective single-stage-to-orbit (SSTO) vehicle has been postponed indefinitely (possibly, for the next couple of decades), partly due to forbidding costs and limited direct investment in aerospace vehicle research and development and partly due to current technology limitations.

However, interest in space access continues to grow due to its future scientific and economic potential. Major space agencies and private corporations are continuously investing resources in associated research and future technologies that will enable the design of the space vehicle of the future. A survey of the current state of the public space sector confirmed the following:

1) A current emphasis on large launch vehicles optimized for launching heavy communication satellites into geostationary transfer orbit or designed for high-mass transport to low Earth orbit.

2) Emergence of new markets for satellites, downstream services, and user equipment.

3) A projected need for 30 geosynchronous-Earth-orbit (GEO) commercial satellite launches per year over the next decade.

4) A steady growth of small-satellite (under 500 kg) launches, which indicates a solid presence of small payloads in the future commercial satellite market.

Overall, there is an increasing interest in small-payload development and deployment within the commercial space market, largely dominated by heavy launchers. Furthermore, the ever-increasing development of nanotechnology provides a solid basis for such predictions.

However, it is currently very difficult to find an economically feasible launch alternative for such relatively small satellites, which do need a specific, low Earth orbit. Typical examples are small science missions, Earth-observation missions, store-and-forward missions, and low-cost technology-demonstration missions.

In the past, satellites falling in any of the preceding categories could be launched with the Solid Controlled Orbital Utility Test (SCOUT) launch system developed by NASA in 1959. The SCOUT, which is no longer in production, was a four-stage solid-propellant launch vehicle capable of launching individual 150- to 300-kg satellites to lower Earth orbits. The only other alternative for an individual launch is provided by the Pegasus air-launch system developed by the Orbital Sciences Corporation. Pegasus is a three-stage solid-propellant launch vehicle launched at an altitude of 12,000 m by an L-1011 carrier aircraft. The launch record, however, is not remarkable. In general, small payloads travel piggyback with another large satellite, generally resulting in a nonoptimal orbit. Hence, there is inevitably a strong dependency on the schedule of the larger satellite, which increases the cost of the small-satellite mission.

The goal of this research program is to produce reliable and accurate design methodologies for the preliminary design of a concept vehicle that would fill the existing technology gap between current launchers and future concepts, by providing an interim realistic and feasible solution that would support current space shuttle operations by enabling fast and potentially economically viable small-payload delivery to space.

II. Vehicle Concept and Mission Profile

The proposed space transportation system is a dual-propulsion uninhabited vehicle with horizontal-takeoff-and-landing capabilities. The key operating principle of the proposed concept is the ability to start the rocket-powered ascent at a high altitude and supersonic Mach conditions while benefiting of the high specific impulse of airbreathing propulsion in the lower regions of the atmosphere. The aim of this operational approach is to reduce the amount of onboard rocket propellant required to achieve orbital velocity and hence improve the payload-delivery performance. Furthermore, the addition of airbreathing propulsion substantially enhances the vehicle's low-level-transit operations. The ability to take off and land horizontally, as well as to encompass powered flyback to alternate landing sites, would provide the proposed system with an unprecedented degree of flexibility. Some of the advantages of this inherent capability are, among others, the ability to disassociate payload-loading sites with launch locations, wider reentry windows, and subsequent turnaround improvements.

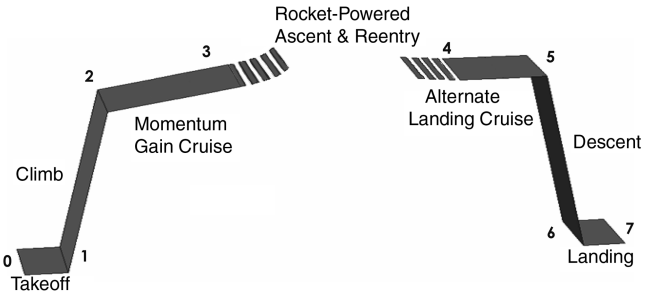

Fig. 1 Mission profile.

The mission profile (Fig. 1) for this vehicle is designed around the main vehicle design requirements: to provide high-speed and high-altitude launch conditions and to ensure alternate landing capabilities.

To achieve this objective, the vehicle will take off horizontally (segments 0–1) and climb to a predetermined altitude (segments 1–2), then it will accelerate until it reaches the maximum Mach number limit of the afterburning turbine-based airbreathing propulsion system (segments 2–3). At this point, the vehicle will perform a pitch-up maneuver and ignite the rocket engine, which will power the craft through the upper levels of the atmosphere until it reaches the required orbital height, then it will release the payload or rendezvous with another spacecraft. Once the deployment mission is complete, the vehicle will reenter the atmosphere (segments 3–4). If required, once it reaches the lower-level atmosphere, it will restart the airbreathing engines and fly back (segments 4–5) to an alternative landing site (segments 5–7). As a result, there are two main cruise segments. The first one (momentum gain cruise) consists of an airbreathing acceleration segment in which the vehicle gains momentum through the atmosphere until it reaches maximum speed, then it performs a pitch-up maneuver to prepare for rocket ignition. The second cruise (alternate landing cruise) commences after atmospheric reentry. For sizing-calculation purposes, the transition between airbreathing and rocket propulsion is simplified by assuming that at the end of the pitch-up maneuver, the aircraft has reached its maximum available kinetic energy, and therefore no overlap of the two propulsion systems takes place. Although this simplification is acceptable at this stage, optimization of the propulsive coupling between the airbreathing engine and rocket should be included in a more extensive future performance analysis to yield the optimum flight conditions for rocket takeover.

The baseline configuration of the proposed concept is based on an equivalent configuration formed by an axisymmetric fuselage with an ogive nose and delta-shaped wings and fins. The rocket's propulsion system is located at the back end of the fuselage, and the airbreathing engines are located under the fuselage after the nose section. Upon reentry, the vehicle flies upside down, with the airbreathing engines guarded from the high temperatures by the thermally protected topside of the vehicle. A protective mechanism is required to cover the inlet in high-speed flight segments. The use of an equivalent configuration throughout the methodology provides the flexibility to perform numerous trade studies easily, while enabling the designer to later develop the actual vehicle geometry from the equivalent configuration.

Furthermore, due to the aircraft-type nature of the proposed aerospace vehicle, it is desired to approach the development of the

design methodologies from the aircraft standpoint and integrate the tools and methods inherent to launch-vehicle design within the overall process. Consequently, the new design synthesis consists of a combination of existing methodologies traditionally used in the aircraft design sector, together with specialized methodologies that are linked to space systems.

III. Initial Sizing Methodology

The most immediate task in the design process is to determine the takeoff gross weight, fuel weight, and propellant weight required for the new concept to perform its design mission.

Traditionally, the takeoff gross weight W_0 is defined as the total weight of the aircraft at the beginning of the mission, and its maximum design value is taken as the maximum takeoff weight (MTOW) during the sizing calculations. The MTOW is the sum of the general aircraft weight components: the payload weight, the rocket-engine weight, the propellant weight, the fuel weight, and the aircraft's remaining empty weight. Equation (1) summarizes the design takeoff weight buildup:

$$W_0 = W_{\text{payload}} + W_{\text{rocket}} + W_{\text{propellant}} + W_{\text{fuel}} + W_{\text{empty}} \tag{1}$$

A distinction was made between rocket-propellant weight and the airbreathing-engine-fuel weight. If the propellant required for orbit injection is calculated, the vehicle's fuel fraction can be estimated using sizing methodologies traditionally used in aircraft design. In addition, the rocket engine is considered as an independent component and its weight has been excluded from the vehicle's empty weight. This approach is desired to maintain the conventional aircraft-sizing-calculation method. The weight of the propellant and rocket engine can be considered as "vehicle-dependent payload" and are calculated separately. By expressing the weight of the empty aircraft and fuel as fractions of the MTOW, Eq. (2) can be rearranged for an iterative solution of W_0:

$$W_0 = \frac{W_{\text{payload}} + W_{\text{rocket}} + W_{\text{propellant}}}{1 - (W_{\text{fuel}}/W_0) - (W_{\text{empty}}/W_0)} \tag{2}$$

A. Empty-Weight Fraction and Rocket-Engine Weight

The empty-weight fraction can be estimated statistically from historical trends. A logarithmic relationship between W_{empty} and W_0 suggested by Roskam [1] is used to estimate the aircraft's empty weight:

$$\log W_{\text{empty}} = \left(\frac{1}{B}\right) \log W_0 - \left(\frac{A}{B}\right) \tag{3}$$

where A and B are the constants of the regression line.

Many efforts were made to obtain weight data from existing and conceptual vehicles (Table 1) of similar configuration characteristics such as reusability, wing geometry, or payload weight.

A linear fit determines the value of the regression-line constants. To further corroborate the accuracy of the set of logarithmic empty and takeoff weights, a correlation analysis is carried out. Using the information presented earlier, the final logarithmic relationship is

$$\log W_{\text{empty}} = (0.798) \log W_0 - (0.412) \tag{4}$$

The resulting correlation factor is 0.974.

The rocket-engine weight was calculated using the same technique, based on a statistical analysis carried out on the properties of existing liquid-propellant rocket engines (LOX/Kerosene, LOX/LH2, and N2O4/UDMH). It was found that a better correlation (0.96) can be achieved by calculating the rocket-engine weight as a function of maximum thrust and the vehicle's takeoff weight. Equations (5) and (6) represent the logarithmic relationships obtained through regression analysis:

$$\log T_{\max} = (0.928) \log W_0 - (1.451) \tag{5}$$

$$\log W_{\text{rocket}} = (0.778) \log T_{\max} - (0.728) \tag{6}$$

B. Fuel-Fraction Weight

Raymer [2] and Roskam [1] provided a technique based on estimating the change in weight across each of the segments that compose the mission profile. The methodologies involved in the weight-fraction calculation are based on a combination of historical trends, analytical equations, and semi-empirical data, but in several cases, an important number of assumptions need to be made for those parameters that are not defined in the design requirements.

The ratio of the aircraft weight at the end of the mission over the initial weight at takeoff can be calculated from the product of the individual weight fractions of all the segments. The total mission weight fraction W_x/W_0 can then be used to estimate the fuel fraction, assuming a typical 6% allowance for reserve and trapped fuel.

Total mission weight fraction:

$$\frac{W_x}{W_0} = \Pi_{i=1}^{n} \frac{W_i}{W_{i-1}} \tag{7}$$

where n is the number of segments. The fuel fraction is therefore

$$\frac{W_{\text{fuel}}}{W_0} = 1.06\left(1 - \frac{W_x}{W_0}\right) \tag{8}$$

C. Propellant Weight

1. Ascent Trajectory

Standard design methodologies [3] used in the sizing of conventional launch vehicles solve this problem by crudely estimating the propellant weight as a function of the vehicle's velocity losses (ΔV). However, the proposed concept relies on two modes of propulsion to accomplish two mission objectives and therefore on two types of fuel (or propellant). Therefore, a second main driving parameter is introduced in the sizing calculations. Furthermore, the weights of both propulsive fuels are dependent on one another. Hence, any inaccuracies introduced in the calculation of any one of them will decrease the precision in the calculation of the other. The initial guess of propellant weight is estimated by calculating the change of mass due to the change of velocity ΔV required to attain the target orbital height, according to the following equation:

Table 1 Weight data for existing and conceptual vehicles

Aircraft	Company	W_0, kg	W_{empty}, kg
X-33	NASA	123,831	28,576
VentureStar	Lockheed Martin	Lockheed Martin	116,573
Black Horse Pathfinder	Pioneer Rocketplane	120,202	27,216
Eclipse Astroliner	Kelly Space & Technology	319,902	95,970
Alchemist	Andrews Space & Technology	673,226	134,645
Pegasus	Orbital	23,133	8117
HOTOL	Rolls Royce/British Aerospace	113,398	22,680

$$\frac{M_{\text{final}}}{M_{\text{initial}}} = \exp\left(\frac{-\Delta V}{I_{\text{SP}}}\right) \tag{9}$$

However, to ensure the reliability of the result, the sizing methodology required a more detailed analysis of propellant estimation. To take into account the atmospheric flight regime in the vehicle's ascent to orbit, the vehicle is represented as a point mass and assumed to describe a planar trajectory over a nonrotating spherical planet. Numerical integration of the governing equations of motion due to the forces exerted on the body provides a simplified trajectory calculation that enables the estimation of the weight of propellant required to reach the target orbit. A second-order Runge–Kutta integration routine is employed to achieve accurate results while maintaining computational efficiency, which is an important factor for rapid-sizing studies [4]:

$$\frac{\mathrm{d}V}{\mathrm{d}t} = \frac{T\cos\alpha - D}{m} - \sin\gamma\left[g - \frac{V^2}{(h+R)}\right] \tag{10}$$

$$\frac{\mathrm{d}\gamma}{\mathrm{d}t} = \frac{T\sin\delta + L}{Vm} - \cos\gamma\left[\frac{g}{V} - \frac{V}{(h+R)}\right] \tag{11}$$

Knowledge of the propulsive and aerodynamic forces experienced by the vehicle is required to solve Eqs. (10) and (11).

2. *Simplified Propulsion Characteristics*

To simplify the calculation of the propulsive characteristics of the vehicle during ascent, the rocket is assumed to operate at a constant throttle setting. The thrust supplied by the rocket can then be calculated using the definition of specific impulse [5]:

$$I_{\text{SP}} = \frac{T}{\dot{m}g} \tag{12}$$

where the value of the rocket's specific impulse I_{SP} is determined according to the type of propellant used. The second unknown in the equation is the rate at which the propellant is burned during rocket operation ($\dot{m}$). This property is normally determined during the design of the engine and, as such, is dependent on many intrinsic parameters for a given rocket. A statistical analysis carried out on the properties of existing rocket engines provided a logarithmic relationship between propellant burn rate and maximum thrust:

$$\log(\dot{m}) = 1.0094 \times \log(T_{\max}) - 0.5164 \tag{13}$$

Combining Eqs. (5) and (13), the propellant burn rate can be estimated for a given vehicle weight at rocket ignition.

3. *Simplified Aerodynamic Calculation*

During the ascent trajectory, the drag of the vehicle can be obtained by calculating the parasite drag coefficient C_{Do} for the given flight condition. However, this approach requires a more detailed knowledge of the geometric configuration of the aircraft. To obtain accurate values of C_{Do}, certain geometric parameters of the vehicle, such as reference wing area and wetted area, must be calculated. To do so, some design methodologies that are normally found outside the initial sizing design loop must be included within.

4. *Design Point Estimation*

The vehicle's wing loading W/S and thrust-to-weight ratio T/W are the two design parameters that always have a major impact on the performance of an aircraft. An unrealistic approximation of these parameters at the initial stages could necessitate a complete redesign of the aircraft in the subsequent stages of the design analysis. It is therefore essential that the estimate of these two variables is both accurate and reliable before proceeding to any further design calculations.

A graphical method is presented by Roskam [1] and Raymer [2] that allows for a rapid estimation of the wing loading and thrust-to-weight ratio by overlaying a set of performance requirements and hence determining the right combination of T/W and W/S that satisfies them all.

The performance objectives consist of 1) stall speed, 2) landing-field length, 3) takeoff-field length, 4) absolute ceiling, 5) cruise speed, 6) maneuvering, and 7) specific excess power.

Each objective provides a set of wing-loading curves as a function of thrust-to-weight ratio and other variables related to that requirement. By plotting these curves (Fig. 2), it is possible to pinpoint the best combination of the highest possible wing loading and the lowest allowable thrust loading (i.e., the design point) that satisfy all of the specified performance requirements.

The procedure employed to automate the graphical technique is described in Fig. 3 and follows the subsequent steps:

1) Calculate the maximum wing loading for the required stall speed.

2) Calculate the lower and upper margins of wing loading for the minimum and maximum landing lift coefficients.

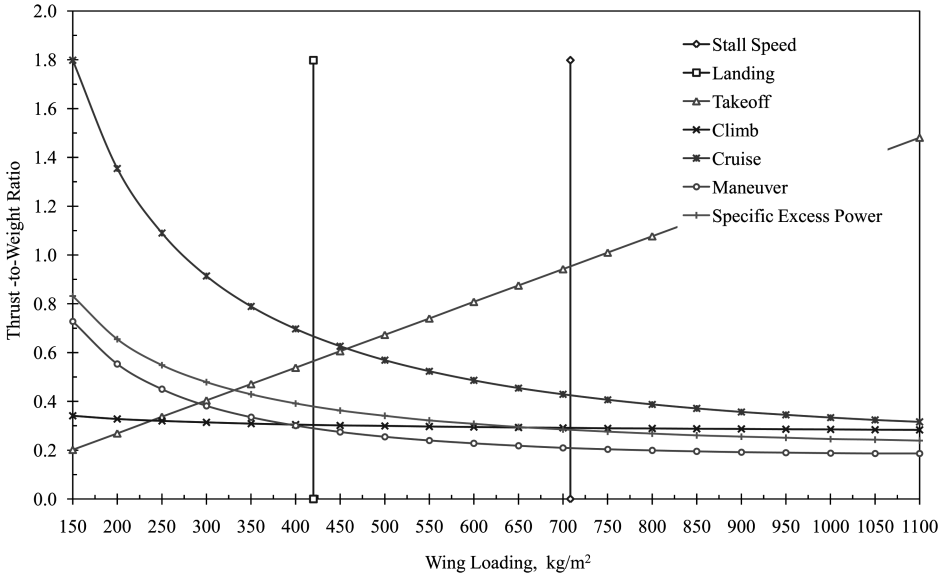

Fig. 2 Example of a performance requirements plot.

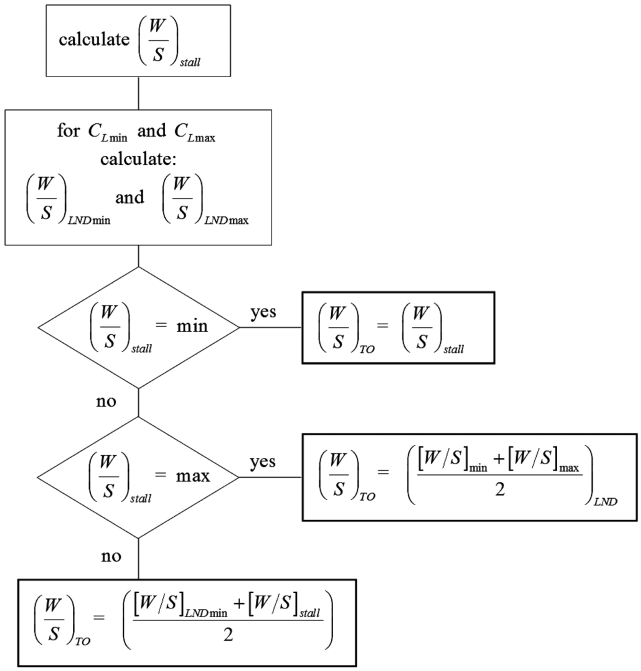

Fig. 3 Flowchart for the estimation of the optimum wing loading.

3) Determine the design wing loading as the average of the two lowest W/S values, while ensuring that the stall-speed requirement is satisfied.

4) Calculate the value of the thrust-to-weight ratio for the remaining performance objectives.

5) Determine design thrust loading as the average of the two highest T/W values.

5. *Equivalent Geometric Configuration*

Once the design point has been selected, the vehicle's reference wing area S_{ref} and takeoff thrust can be established. Furthermore, aerodynamic and performance variable targets are established by reversing the methodology.

Once the reference wing area has been established, the remaining geometric characteristics can be calculated for the vehicle's equivalent configuration. This involves defining the shape of the main components (such as aerodynamic surfaces, fuselage, and engines) as well as calculating the wetted area of the overall configuration.

The process followed for each of the main components is the following:

1) Calculate the significant variables that define the shape of the component.

2) Represent the component as a matrix of coordinates in three-dimensional space.

3) Calculate the area of each polygon in the 3-D coordinate matrix.

4) Calculate the total wetted area of the component from the sum of the polygon areas.

The geometric representation of each of the components results in the development of an equivalent configuration of the vehicle, which enables an early estimation of the center of gravity and a quick visual illustration of the vehicle.

6. *Parasite-Drag-Component-Buildup Method*

The drag analysis carried out on the vehicle mainly focuses on the calculation of the parasite drag coefficient C_{Do}. Once the variation of the zero-lift drag with Mach number for a given flight altitude has been calculated, the total drag can be found as a function of the vehicle's lift coefficient. If we assume steady-state flight, the lift coefficient can be calculated for the given flight condition. Raymer [2] provides a rapid estimation procedure for calculating the parasite drag coefficient of a vehicle throughout the subsonic and supersonic flight regimes. It is based on a conventional component-buildup method and involves the computation of skin friction coefficients, as well as form and interference factors for each major aircraft component.

In the subsonic regime, the parasite drag coefficient of the aircraft is estimated as the sum of the preceding for each component plus any miscellaneous, leakage, and protuberance drag contributions [Eq. (14)]:

$$C_{\text{Do}} = \frac{\Sigma(C_{f_c} FF_c Q_c S_{\text{wet}_c})}{S_{\text{ref}}} + C_{D_{\text{misc}}} + C_{D_{l\&p}} \tag{14}$$

The supersonic parasite drag can be calculated using a similar approach as that for subsonic flight. The main differences are that the form or interference factors are not included in the component's parasite-drag estimation and that an extra term must be added to account for the presence of wave drag:

$$C_{D_0} = \frac{\Sigma(C_{f_c} S_{\text{wet}_c})}{S_{\text{ref}}} + C_{D_{\text{misc}}} + C_{D_{l\&p}} + C_{D_{\text{wave}}} \tag{15}$$

Wave drag is the main contributor to the aircraft's parasite drag in the supersonic flight regime. As mentioned earlier, it is a result of a pressure variation induced by shocks, and it is directly related to the volume distribution of the aircraft. The wave drag at Mach 1.0 is minimized when the aircraft's volume distribution is identical to that of a Sears–Haack body:

$$\frac{r}{r_{\max}} = \left[1 - \left(\frac{x}{l/2}\right)\right]^{0.75} \tag{16}$$

To calculate the wave drag accurately, it would be necessary to use a simplified computer version of the widely used Harris wave drag code. However, to perform a preliminary analysis, the wave drag of the aircraft for $M_0 \geq 1.2$ can be related to that of a Sears–Haack body by

$$(D/q)_{\text{wave}} = E_{\text{WD}}\left[1 - 0.36(M_0 - 1.2)^{0.57} \times \left(1 - \frac{\pi \Lambda_{\text{LE}_{\text{deg}}}^{0.77}}{100}\right)\right]\left(\frac{D}{q}\right)_{\text{Sears–Haack}} \tag{17}$$

$$\left(\frac{D}{q}\right)_{\text{Sears–Haack}} = \frac{9\pi}{2}\left(\frac{A_{\max}}{l}\right)^2 \tag{18}$$

where l represents the fuselage length minus any section with a constant cross-sectional area, and Λ_{LE} is the wing leading-edge sweep angle

The empirical term E_{WD} is the ratio of the actual wave drag to the minimum possible wave drag (Sears–Haack) and relates to the wave drag efficiency of the aircraft. The value of E_{WD} can be minimized by ensuring a smooth volume distribution. For a well-designed supersonic vehicle, the value of E_{WD} may be as low as 1.2. Although Roskam [1] suggests a value of 1.6 for a supersonic transport, a value of 1.4 is used in the preliminary wave drag calculations on the assumption that fuselage shaping ensures favorable volume distribution.

The transonic regime extends from $M_0 = 0.8$ to 1.2. Linear wave drag methods are not suitable for estimating the drag rise that develops in this regime, due to the formation of shocks. There are two important speeds that help describe the drag behavior in the transonic regime: the critical Mach number M_{CR} and the drag-divergent Mach number M_{DD}. M_{CR} is described as the Mach number at which shocks first start to form on the aircraft. M_{DD} is the Mach number at which the formation of shocks affects drag substantially. The speed at which this occurs is rather arbitrary, and different definitions are used. The Boeing MDD is set when the drag rise reaches 20 counts (0.002), and the Douglas M_{DD} is set when the rate of change of parasite drag with Mach number reaches 0.1.

Without the use of a sophisticated computational fluid dynamics (CFD) package, the drag increase in this region must be approximated graphically. Raymer [2] provides a preliminary estimate of the drag-divergent Mach number through

$$M_{\mathrm{DD}} = M_{\mathrm{DD}_{L=0}} LF_{\mathrm{DD}} - 0.05C_{D_0} \tag{19}$$

where $M_{\mathrm{DD}_{L=0}}$ stands for the wing drag-divergent Mach number for zero lift, and LF_{DD} is the lift-adjustment factor for M_{DD}.

The values for these parameters, which are a function of the wing quarter-chord sweep and thickness-to-chord ratio, respectively, are estimated from charts [2]. Because the Mach number is directly dependent on the lift coefficient of the aircraft, it would be necessary to calculate the drag-divergent Mach number for each point in the mission. However, for initial analysis, a single value of M_{DD} for the midcruise weight and altitude is sufficient.

With the evaluated M_{DD}, the increase in wave drag throughout the transonic regime can be estimated graphically by interpolating the parasite drag for certain Mach numbers:

1) M_{CR} is roughly 0.08 lower than M_{DD}.

2) The drag at $M = 1.05$ is typically equal to the drag at $M = 1.2$.

3) The drag at Mach 1.0 can be approximated as half of that at Mach 1.05.

By joining these points with the subsonic and supersonic wave drag values (calculated previously) with a smooth curve, the parasite-drag variation with Mach number can be estimated for any given altitude.

D. Integration

Figure 4 shows the structure of the proposed sizing methodology. The highlighted blocks (rounded edges) represent the methods added to the conventional sizing routine, traditionally linked to aircraft design, to account for the orbital characteristics of the mission. As a result of the introduction of these methods, the results obtained at this early stage not only include an estimation of vehicle weights, but also consist of sufficiently accurate estimations of aerodynamic characteristics, vehicle component geometries, and performance targets. These initial values provide a reliable starting point in the subsequent design steps, thus ensuring fast and consistent design iterations (I stands for iteration loop and C stands for convergence).

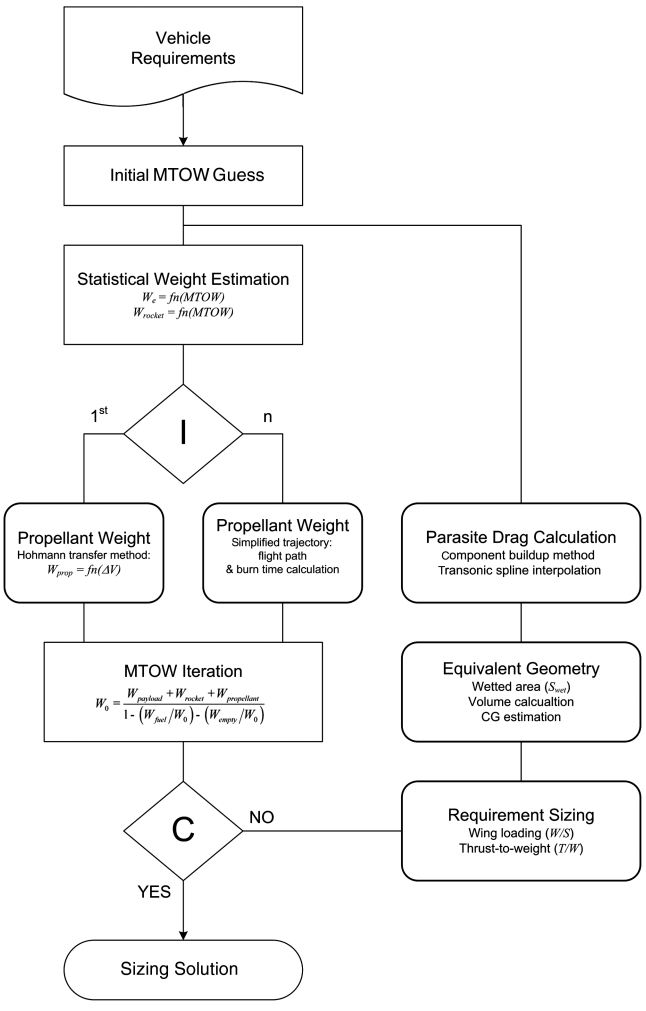

Fig. 4 Proposed initial sizing methodology.

IV. Trajectory

Both the energy-state approximation (ESA) method and optimal control theory have been shown to produce good results for the trajectory optimization problem [6,7]. However, the system of differential equations that results from the application of optimal control theory presents a two-point-boundary-value problem. Because of the nature of the method, the equations can present multiple roots and *are always half-unstable*. Although well-established numerical techniques have been developed to solve this problem, the resulting methods are not robust enough and tend to be too computationally intensive and hence inappropriate for integration in conceptual design synthesis tools [8]. The use of energy-based equations to determine the flight and maneuverability performance of conventional aircraft designs is an established approach [2,9]. Furthermore, the technique has been successfully implemented in the trajectory optimization of both the ascent and descent phases of launch vehicles [10–16]. For these reasons, the ESA method was chosen for developing the ascent and descent methodologies.

According to the ESA model, the minimum time-to-climb trajectory for a given aircraft can be determined by calculating the maximum excess power along curves of constant energy heights. Furthermore, the energy equations can be further modified to account for the minimization of other parameters such as fuel-specific energy [2] or maximum heat load [12]. Hence, solving for any combination of Eqs. (20–22), a near-optimal trajectory can be calculated for any of the required parameters.

Minimum time to climb:

$$f = \int_{h_{e_0}}^{h_{e_f}} P_s \, \mathrm{d}h_e \tag{20}$$

Minimum fuel:

$$f' = \int_{h_{e_0}}^{h_{e_f}} \frac{f_s}{P_s} \, \mathrm{d}h_e \tag{21}$$

Minimum heat load:

$$f' = \int_{h_{e_0}}^{h_{e_f}} \frac{T_{\mathrm{surf}}^4}{P_s} \, \mathrm{d}h_e \tag{22}$$

The governing equations of motion considered in the numerical calculations are based on a point-mass vehicle simplification over a spherical rotating Earth with no winds aloft [Eqs. (23–28)]. The square of the terms resulting from the Earth's rotation are neglected.

$$\dot{X} = \frac{VR\cos\gamma\cos\chi}{(h+R)\cos(Y/R)} \tag{23}$$

$$\dot{Y} = \frac{VR\cos\gamma\sin\chi}{(h+R)} \tag{24}$$

$$\dot{h} = V\sin\gamma \tag{25}$$

$$\dot{V} = \left[\frac{T\cos(\alpha+\delta) - D}{m}\right] - g\sin\gamma \tag{26}$$

$$\dot{\gamma} = \left(\frac{L}{mV}\right)\cos\phi + \frac{T\sin(\alpha+\delta) - D}{mV} - \frac{g}{V}\cos\gamma + \frac{V}{(h+R)}\cos\gamma + 2\omega\cos\chi\cos\frac{Y}{R} \tag{27}$$

$$\dot{\gamma} = \left(\frac{L}{mV\cos\gamma}\right)\sin\phi + \left[\frac{T\cos(\alpha+\delta)}{mV\cos\gamma}\right] - \frac{V}{(h+R)}\cos\gamma\cos\chi\tan\frac{Y}{R} + 2\omega\left(\tan\gamma\sin\chi\cos\frac{Y}{R} - \cos\frac{Y}{R}\right) \tag{28}$$

The ESA model relies on minimizing a given cost function for different combinations of the vehicle's altitude and Mach number along curves of constant specific energy. To minimize the number of calculations along curves of constant energy height, the flight envelope is restricted by boundaries determined by dynamic pressure limits. Once the number of constant energy curves has been chosen, the numerical searches are made by dividing the allowable altitude range at each energy level into a large number of steps and calculating the value of the function to be minimized at each point.

The first step is based on setting up the trajectory envelope based on curves of constant specific energy and bounded by the constraints imposed by dynamic pressure and minimum and maximum altitudes (if considering reentry trajectories). The result is a cloud of Mach number and altitude combination points (Fig. 5) that encompass all possible trajectory paths.

The second step involves the calculation of the aerodynamic characteristics of the vehicle's configuration for all of the altitude/Mach-number combinations throughout the envelope. Lift and drag coefficients were obtained through the integration of Digital and Missile DATCOM. The solutions obtained from Missile DATCOM [17,18] were mostly used during the orbital and reentry segments, due to its suitability over a wide range of Mach numbers and angles of attack [19]. On the other hand, Digital DATCOM [20–22] was used to calculate the vehicle's characteristics during aircraft-type operations that generally take place at lower Mach numbers and less severe angles of attack. For reentry trajectories, the allowable angle of attack was set within −45 and +45 deg [16].

Figure 6 describes the implementation of the ESA method in the design and optimization of ascent and/or descent trajectories.

Once the envelope has been established and the aerodynamic and propulsive performance has been calculated, the data can be accessed repeatedly to calculate trajectories for different optimization criteria. The numerical search for the local maximum along a curve of constant specific energy is achieved by calculating the value of the function of interest at each altitude and Mach number combination along the energy height. For a given altitude step, the lift coefficient required to satisfy the equations of motion can be determined by solving for Eq. (27). For this value of C_L, the corresponding angle of attack can then be interpolated from the tabular data provided by the DATCOM calculation module followed by the corresponding drag coefficient. As a result, the vehicle's specific excess power for the corresponding combination of altitude and velocity is calculated.

The next step involves the estimation of the time interval between the current altitude and the previous altitude, corresponding to the maximum solution along the previous energy height:

$$\Delta t = \frac{h_e|^n - h_e|^{n-1}}{|(P_s|_i^n - P_s|_{\max}^{n-1})/2|} \tag{29}$$

where i refers to an altitude step along a specific energy curve n.

Once the value of the optimizing function has been determined for all of the altitude steps along the energy curve, the local maximum is selected and the process is repeated along the remaining energy heights. The collection of calculated local maxima along the energy curves throughout the envelope provides the near-optimal trajectory.

To calculate the transient surface temperatures and heat-rate values n for each of the altitude steps in the trajectory envelope, an aeroheating prediction technique was incorporated in the trajectory optimization process.

V. Aeroheating and Thermal Protection System Sizing

High-fidelity numerical simulation codes and techniques are capable of producing extremely precise heat-flux solutions "as well as the interactions between inviscid and viscous flow regions due to heat transfer and entropy-layer swallowing" [23] for very detailed geometries. However, all of these methods are computationally intensive [24], requiring long computer run times for all but the simplest geometries. With this in mind, it is important to consider that the definition of the aerothermal environment at the preliminary design stage might consist of a flight-profile matrix of Mach number,

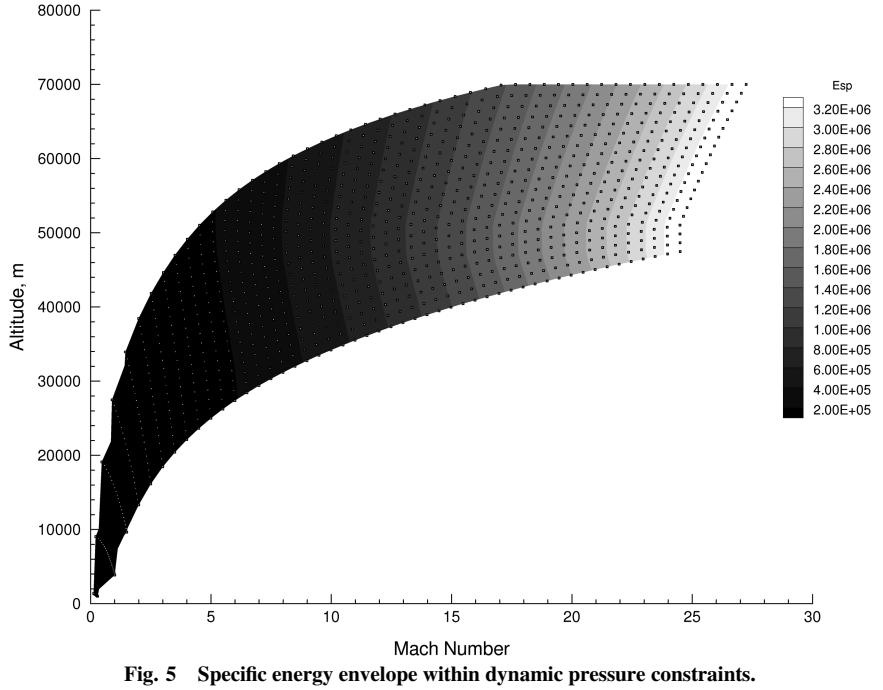

Fig. 5 Specific energy envelope within dynamic pressure constraints.

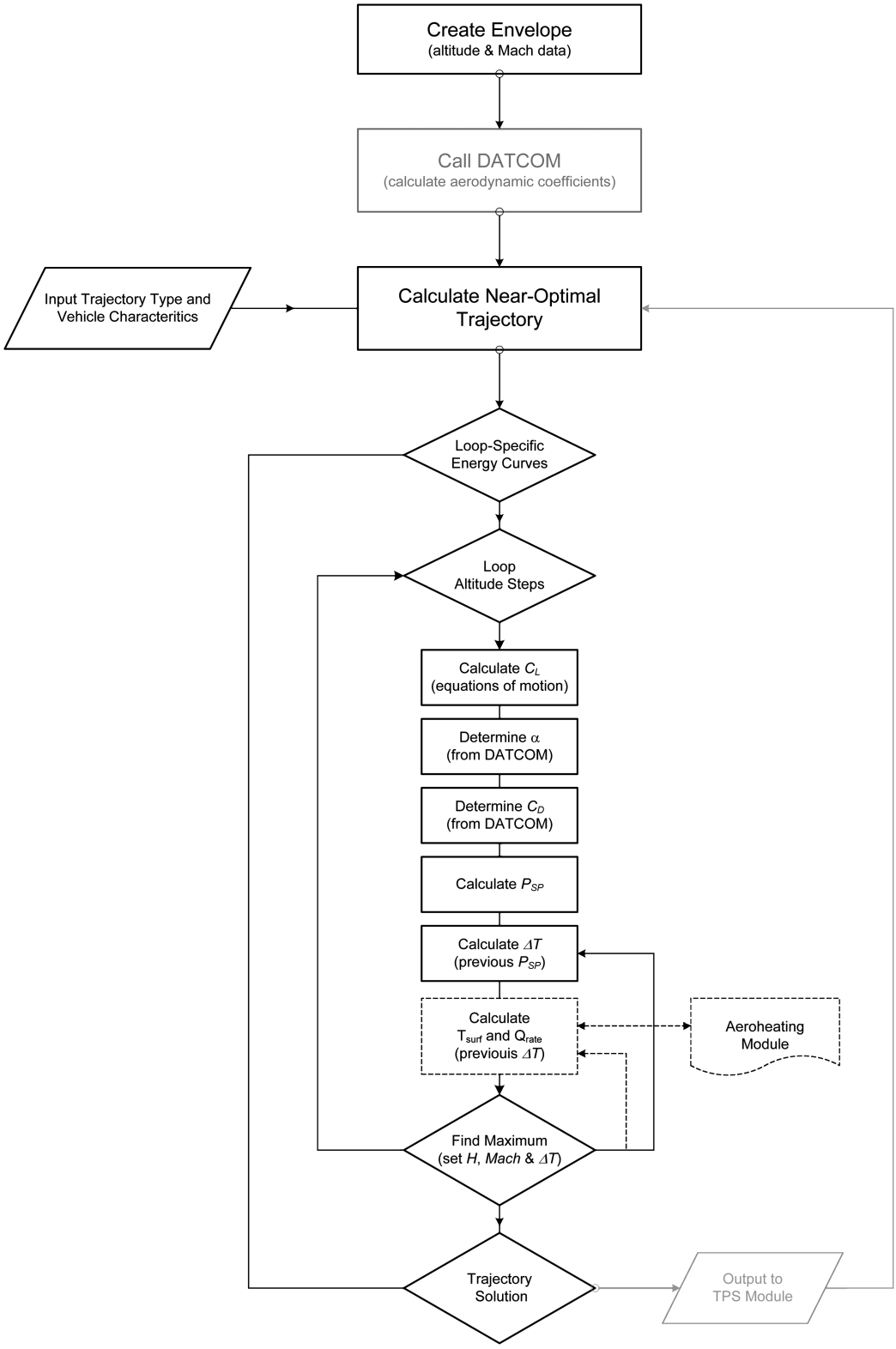

Fig. 6 Proposed trajectory methodology.

altitude, and angle of attack, spanning through as many as 8000 cases ($25 \times 16 \times 20$). One must conclude that the use of computational fluid dynamics for all of these cases is not appropriate. The requirement for accuracy must be balanced against the need for speed and flexibility.

For this reason, the use of CFD simulations is typically confined to the later stages of the design process, and specialized engineering codes are employed in the early design phase to provide the aerothermal databases.

For these reasons, a slightly simplified version of the semi-empirical methods employed in the engineering code TPATH [23] was used as the basis of the aeroheating methodology to predict stagnation temperatures and heat rates. Based on the earlier work by Quinn and Gong [25], it uses semi-empirical theories to calculate laminar and turbulent heat transfer coefficients. In turn, these are used to predict three-dimensional stagnation heating rates and temperatures, as well as two-dimensional stagnation heating rates and temperatures with and without leading-edge sweep. The

program is also capable of determining lower- and upper-surface heating rates and transient surface temperatures for flat plates, wedges, and cones.

The equation used to compute the heating rates and surface temperatures for stagnation points is based on the time rate of change of heat stored in a thin-skin element [26].

For three-dimensional stagnation points and two-dimensional points without sweep:

$$q = (\rho_w \;\; C_{P,w} \;\; \tau)\frac{\mathrm{d}T_w}{\mathrm{d}t} = C_h(H_{\mathrm{st}} - H_w) - \beta T_w^4 + S \tag{30}$$

For two-dimensional points with sweep:

$$q = (\rho_w \;\; C_{P,w} \;\; \tau)\frac{\mathrm{d}T_w}{\mathrm{d}t} = C_h(H_R - H_w) - \beta T_w^4 + S \tag{31}$$

Note that the S term in Eqs. (30) and (31) is the heat input due to solar and nocturnal radiation. This term is negligible and normally set to zero. More important, both equations are a function of the heat transfer coefficient.

For three-dimensional stagnation points, the heat transfer coefficient is calculated using a modified version of the method of Fay and Riddell [27]:

$$C_h = 0.94K_1(\rho_{\mathrm{st}} \;\; \mu_{\mathrm{st}})^{0.4}(\rho_w \;\; \mu_w)^{0.1}\sqrt{\left(\frac{\mathrm{d}u}{\mathrm{d}x}\right)_{x=0}} \tag{32}$$

For two-dimensional points with or without sweep, the heat transfer coefficient was given by Beckwith and Gallagher [28] as

$$C_h = 0.704K_2(\rho_{\mathrm{st}} \;\; \mu_{\mathrm{st}})^{0.44}(\rho_w \;\; \mu_w)^{0.06}\sqrt{\left(\frac{\mathrm{d}u}{\mathrm{d}x}\right)_{x=0}} \tag{33}$$

To calculate the solutions to the preceding equations, the local flow conditions behind a normal shock wave and at the edge of the boundary layer must be determined. Values of the velocity, enthalpy, and pressure behind the normal shock could be computed using the real gas solution developed by Moeckel [29]. However, Quinn and Gong [25] suggested a method that uses only the freestream conditions and values of predetermined stagnation heating factors K_1 and K_2, to minimize computational time while providing adequate solutions. The stagnation enthalpy for three-dimensional flows and two-dimensional flows without sweep is given by

$$H_{\mathrm{st}} = H_\infty + \frac{V_\infty^2 \cos^2 \Lambda}{2gJ} \tag{34}$$

For two-dimensional flows with sweep, the recovery enthalpy is calculated as

$$H_R = H_\infty + \frac{V_\infty^2}{2gJ} + 0.855\frac{V_\infty^2 \sin^2 \Lambda}{2gJ} \tag{35}$$

The stagnation velocity gradient is determined for both flows from the following equation:

$$\left(\frac{\mathrm{d}u}{\mathrm{d}x}\right)_{x=0} = \frac{1}{R}\sqrt{\frac{\left(7M_\infty^2\cos^2\Lambda - 1\right)\left(M_\infty^2\cos^2\Lambda + 5\right)}{M_\infty^2\cos^2\Lambda}\left(\frac{p_\infty}{\rho_\infty}\right)} \tag{36}$$

And the flow parameters at stagnation or wall conditions are given by

$$\rho_{\mathrm{st}}\mu_{\mathrm{st}} = \rho_\infty\mu_\infty\left(\frac{6M_\infty^2\cos^2\Lambda}{M_\infty^2\cos^2\Lambda + 5}\right)\left(\frac{T_{\mathrm{st}}}{T_\infty}\right)^{0.75} \tag{37}$$

$$p_w \approx p_{\mathrm{st}} \approx p_\infty\frac{\left(7M_\infty^2\cos^2\Lambda - 1\right)}{6} \tag{38}$$

$$\rho_w = \frac{p_w}{z_w R T_w} \tag{39}$$

The sweep angle Λ is set to zero for three-dimensional calculations. The remaining values of H_∞, H_w, T_R, T_{st}, μ_w, and z_w are calculated by linear interpolation of tabulated data of the thermodynamic properties of real gas in chemical equilibrium obtained from Hansen [30]. Tables and graphs provide the compressibility factors, enthalpy, viscosity coefficients, speed of sound, and Prandtl numbers for air in dimensionless form over an array of temperatures ranging from 500 to 15,000 K and pressures from 0.0001 to 100 atmospheres. An example of the tabulated and graphical data can be found in its appendices.

The integration of the preceding method in the design methodology is achieved by solving Eqs. (30) and (31) for the rate of change of surface temperature throughout a described trajectory. For the three-dimensional flow, the equation becomes

$$\frac{\mathrm{d}T_w}{\mathrm{d}t} = \frac{h(H_{\mathrm{st}} - H_w) - \beta T_w^4}{\rho_w C_{P,w}\tau} \tag{40}$$

with

$$\frac{\mathrm{d}T_w}{\mathrm{d}t} = \frac{h(H_R - H_w) - \beta T_w^4}{\rho_w C_{P,w}\tau} \tag{41}$$

for the two-dimensional case.

Given an initial value of the surface temperature and the altitude and velocity histories, the wall-temperature variation along the trajectory is obtained by numerically integrating Eqs. (40) and (41) using a fourth-order Runge–Kutta algorithm [31].

The heat-capacity term $\rho_w C_{P,w}\tau$ is a function of the thermal properties of the surface material and its thickness. Hence, to obtain the solutions to Eqs. (30) and (31), the properties of the thermal protection system (TPS) material must be known. For a given trajectory and choice of thermal protection system, the heat-flux and surface-temperature histories can be calculated.

To accomplish this, an early version of the thermal-protection-system sizing-tool TCAT was integrated within the trajectory and aeroheating codes. TCAT was developed by Cowart and Olds [32,33] at the Space Systems Design Laboratory at the Georgia Institute of Technology. Designed to be used in the conceptual design environment, it generates 1-D temperature profiles within single- and multilayer TPS material construction using a fully implicit method to solve the parabolic, one-dimensional, unsteady heat-conduction equation by marching in time, and it is also capable of optimizing the material's thickness required to prevent the vehicle's substructure from exceeding its operating temperature limit.

TCAT couples with TPSX, a NASA material properties database, to obtain material properties. Because access to this database is restricted, only a selection of the TPS materials was made available to the authors and these materials are listed in Table 2.

Materials used are either blankets or tiles. Each material is modeled as a TPS material stackup in which the material chosen is the one that is sized. The blanket materials consist of a three-layer

Table 2 TPS materials available to authors

Windward materials	Leeward materials
Shuttle-technology materials	
RCC tiles	RCC tiles
LI-2200 tiles	AFRSI blankets
FRO tiles	FRSI blankets
Next-generation RLV materials	
RCC tiles	CFBI blankets
SiC tiles	AFRSI-2500 blankets
TUFI tiles	AFRSI-2200 blankets
	DURAFRSI blankets
Group combination of materials	
RCC tiles	CFBI blankets
SiC tiles	SiC tiles
AETB-12 tiles	AFRSI-2200 blankets
AETB-8 tiles	DURAFRSI blankets
LI-900 tiles	PBI blankets

stackup that includes the blanket insulation, an adhesive, and the backface material. Five materials make up tile configuration: a tile, an adhesive, a strain isolator pad, an adhesive, and the backface material.

TCAT has proven to be reasonably accurate at calculating the TPS unit weights for in-flight trajectories. In addition to this, a restricted version of the code has been developed that improves the numerical accuracy by an order of magnitude through implementation of the Crank–Nicolson method and also expands the program sizing capability to TPS materials above cryogenic fuel tanks for ground hold operations.

VI. Results

To compare the solutions obtained with the proposed methodology with existing vehicles, the initial sizing program was executed for two different configurations of the proposed reusable spaceplane (RSP) concept.

The first configuration (RSP) was assumed to have no flyback capability, whereas the second configuration ($RSP_{flyback}$) included a 500-km flyback range. In both cases, the payload and orbit requirements were chosen to match those of the existing Pegasus XL launch vehicle. Table 3 includes the main parameters chosen for the mission profile, and Table 4 shows the calculated vehicle component weights for the proposed $RSP_{flyback}$ concept.

The solution for both cases is given as a ratio of the payload to the maximum takeoff weight ($W_{payload}/W_0$). This ratio is the standard figure of merit used to describe the performance capability of launch vehicles. The results obtained for both cases are shown in Table 5, in which they are being compared with other launch vehicles of interest in terms of their specifications: VentureStar (reusable SSTO concept), space shuttle (only reusable launch vehicle), and PegasusXL (only small-payload launch vehicle). A comparison of the operational capabilities of four of the preceding vehicles is also shown in Table 5.

Although the payload-to-gross-weight ratio provides a good comparison indicator, it would be desirable to include a cost-per-pound analysis in the future for a more accurate assessment.

Execution of the initial sizing program also produces trajectory solution plots (Fig. 7). Overall, the results obtained show a good comparison with existing vehicles. The payload ratio is considerably better than that of the space shuttle (35% increase) and the RSP configuration without flyback capability is close to the PegasusXL figure of merit (10% difference).

Table 3 Proposed concept main requirements

Launch		
Payload	500	kg
Orbit	380,000	m
Rocket ignition		
Mach	2.5	
Altitude	20,000	m
Flyback capability		
Range	500,000	m
Propulsion		
Turbofan BPR	0.35	
Rocket propellant	LOX/LH2	

Table 4 Weights and design point results

Weights		
$W_{payload}/W_0$	0.014	
W_0	33,221	kg
W_{fuel}	2942	kg
W^*_{empty}	4340	kg
$W_{propellant}$	25,489	kg
Design point		
T/W_{TO}	1.34	
W/S_{TO}	648	kg/m2

Table 5 Launch-vehicle capability comparison

	Shuttle	Pegasus	RSP	$RSP_{flyback}$
$W_{payload}/W_0$	0.011	0.019	0.017	0.014
W_0, kg $\times 10^3$	2041	23	26	33
W_{empty}, kg $\times 10^3$	269.4	3.0	3.5	4.3
$W_{payload}$, kg	23,133	443	450	450
SSTO			×	×
Multistage	×	×		
Flyback				×
LEO	×	×	×	×
ISS	×			
GEO		×	×	×

Although the applicability of DATCOM for conceptual and preliminary design has been satisfactorily established [19,34], due to the nature of reentry trajectories, it is of particular interest to corroborate the accuracy of Missile DATCOM in high-speed and high-angle-of-attack flight regimes Measured aerodynamic data of a typical ascent trajectory of the Pegasus XL are used to compare lift and drag coefficients predicted by DATCOM. The axisymmetric body and clean aerodynamic surfaces of the Pegasus XL launcher share close resemblance to the equivalent configuration calculated by the initial sizing routine, therefore providing an appropriate choice for comparison. The lift and drag coefficients calculated using Missile DATCOM are compared with measured data for the preceding profile in Fig. 8. The geometric representation of the vehicle required as input for the DATCOM code was approximated from Pegasus information available from Orbital Sciences Corporation.[‡]

To validate the aeroheating model, a comparison was made with the solutions obtained by a real-time 6-DOF simulation program for a generic hypersonic vehicle [25]. Figure 9 shows the stagnation heating rates and temperatures from the real-time simulation compared with values calculated by the aeroheating model.

The validity of this method for preliminary design calculations has been further proved by Quinn and Gong [24] by comparing results obtained using the aeroheating model with flight test data from vehicles such as the X-15 research aircraft, the YF-12 airplane, and the space shuttle. Overall, the results are in good agreement with the flight test data, and only a slight overprediction of the surface temperature is observed after touchdown, due to the program's inherent inability to take into account internal cooling processes.

Having validated the applicability of the proposed methods, solutions from the initial sizing analysis presented earlier were used within the trajectory-calculation routine to produce near-optimal trajectories for three cases: minimum time, minimum temperature, and minimum heat load; the solutions are presented in Fig. 10.

The minimum-time trajectory clearly follows the maximum dynamic pressure boundary. With this in mind, if any heating constraints were imposed on the calculation, the solution optimized for minimum time would most likely exceed the temperature limitation. A minimum-temperature trajectory is included in the results to provide a comparison with the near-optimal heat-load trajectory. The trajectory profiles for the proposed concept show that the minimum-heat-load trajectory exhibits an intermediate solution between those of minimum time and minimum temperature, with a closer resemblance to the latter. In fact, the minimum-heat-load trajectory achieves a nearly minimum-temperature profile in a shorter period of time.

VII. Conclusions

A selection of proposed methodologies was presented that would enable the preliminary design of an uninhabited reusable spaceplane

[‡]Data available online at http://www.orbital.com/SpaceLaunch/Pegasus/index.html [retrieved June 2007].

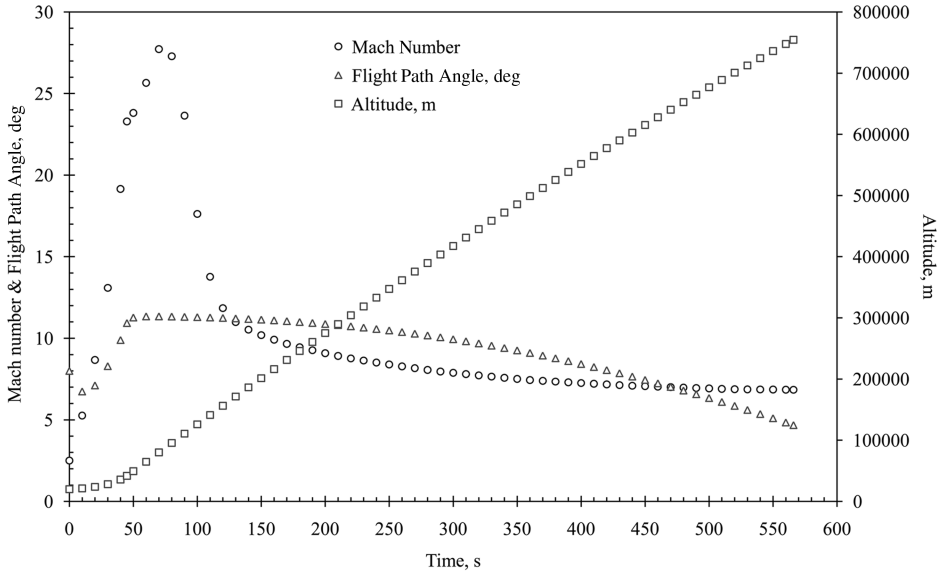

Fig. 7 $RSP_{flyback}$: Mach number, altitude, and flight-path-angle variations with trajectory time.

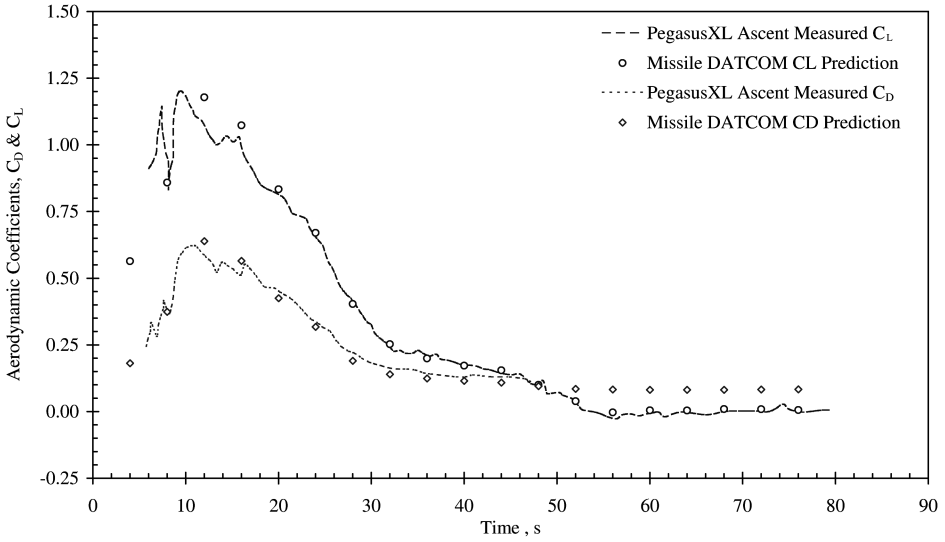

Fig. 8 Validation of Missile DATACOM lift and drag predictions.

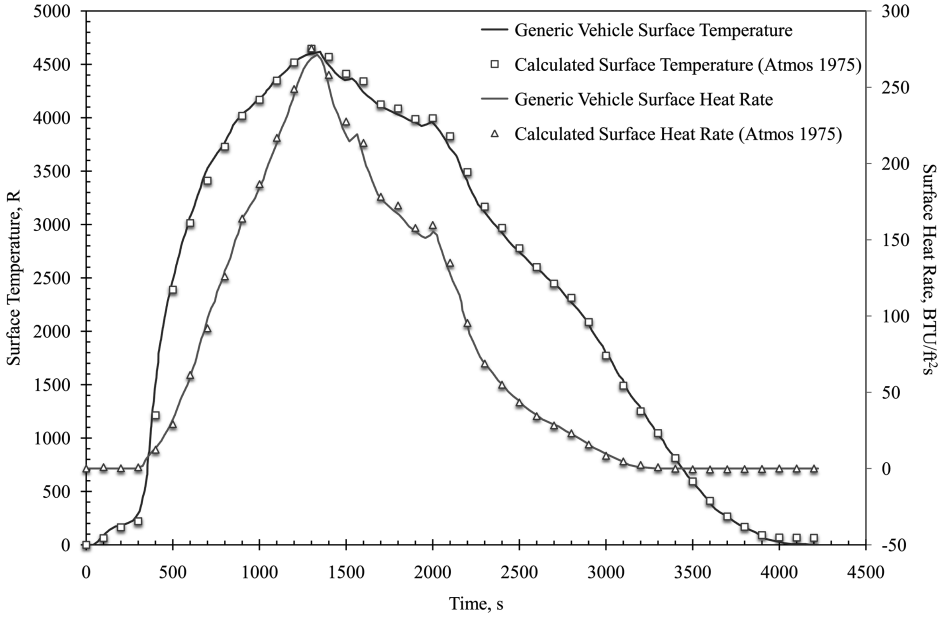

Fig. 9 Three-dimensional stagnation surface temperatures and heating rates.

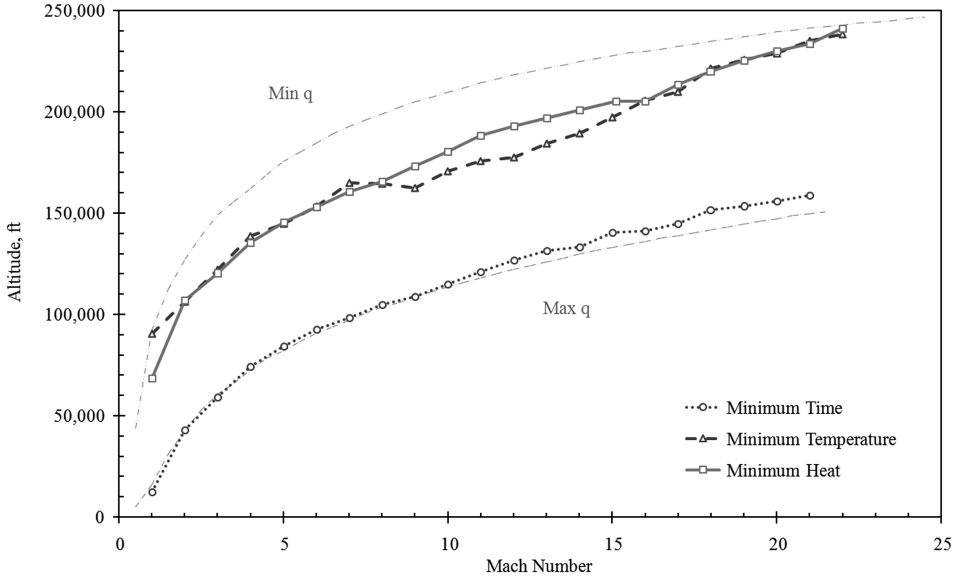

Fig. 10 Minimum time, temperature, and heat reentry trajectories.

capable of delivering small payloads to space. The concept makes use of a combination of airbreathing and rocket propulsion systems, which are used sequentially during the ascent segment of the mission, giving the vehicle a higher rocket ignition altitude and the capability to fly to alternate landing sites upon reentry. In an effort to adhere to the dual nature of the vehicle's operational characteristics, the methodologies presented in the paper have merged traditional aircraft design methods with analysis specific to space vehicle design.

The results obtained from the initial sizing methodology demonstrate the validity of this combined synthesis of traditional aircraft and launch-vehicle-specific methods. More important, a comparison of payload-delivery capability with those of existing and concept launch vehicles further strengthens the feasibility of the proposed design concept. Furthermore, comparison of aeroheating solutions obtained using the presented aeroheating model with other vehicles shows that the surface heating rates and surface temperatures predicted by the heating algorithm are within the accuracy required to evaluate the heating severity of ascent and reentry flight trajectories.

Finally, a trajectory design routine based on the energy-state approximation was proposed to be capable of integrating the thermal heating calculations into the initial design analysis, producing near-optimal ascent and descent trajectories. The ability to further incorporate the thermal-protection-system design-tool TCAT provides the trajectory method with the potential of calculating trajectories optimized for minimum heat load and TPS weight. The possibility of incorporating lifting-reentry optimization is currently being considered to evaluate the impact of such trajectories on surface temperature and heat loads.

The methodologies presented in this paper form part of a continuing research effort toward developing a complete and fully automated design synthesis that will enable designers to generate comprehensive and practical initial design solutions for reusable aerospace vehicles.

References

[1] Roskam, J., *Airplane Design*, Part 1: Preliminary Sizing of Airplanes, Roskam Aviation and Engineering Corp., Ottawa, KS, 1988.

[2] Raymer, D. P., *Aircraft Design: A Conceptual Approach*, 2nd ed., AIAA, Washington, D.C., 1992.

[3] Hammond, W. E., *Design Methodologies for Space Transportation Systems*, AIAA, Reston, VA, 2001.

[4] Press, W. H., *Numerical Recipes in C++: The Art of Scientific Computing*, Cambridge Univ. Press, New York, 2002.

[5] Sutton, G. P., *Rocket Propulsion Elements: An Introduction to the Engineering of Rockets*, 5th ed., Wiley, New York, 1986.

[6] Venugopal, N., Grandhi, R. V., Hankey, W. L., and Belcher, P. J., "Combined Energy Management and Calculus of Variations Approach for Optimizing Hypersonic Vehicle Trajectories," *Computing Systems in Engineering*, Vol. 1, Nos. 2–4, 1990, pp. 591–600.

[7] Hermann, J. A., and Schmidt, D. K., "Fuel-Optimal SSTO Mission Analysis of a Generic Hypersonic Vehicle," AIAA Paper 1995-3372, 1995.

[8] Chou, H.-C., Ardema, M. D., and Bowles, J. V., "Near-Optimal Re-Entry Trajectories for Reusable Launch Vehicles," *Journal of Guidance, Control, and Dynamics*, Vol. 21, No. 6, 1998, pp. 983–990.

[9] Roskam, J., *Airplane Design*, Part 7, Roskam Aviation and Engineering Corp., Ottawa, KS, 1988.

[10] Kremer, J.-P., and Mease, K. D., "Near-Optimal Control of Altitude and Path Angle During Aerospace Plane Ascent," *Journal of Guidance, Control, and Dynamics*, Vol. 20, No. 4, 1997, pp. 789–796.

[11] Corban, J. E., Calise, A. J., and Flandro, G. A., "Rapid Near-Optimal Aerospace Plane Trajectory Generation and Guidance," *Journal of Guidance, Control, and Dynamics*, Vol. 14, No. 6, 1991, pp. 1181–1190.

[12] Sachs, G., and Dinkelmann, M., "Heat Input Reduction in Hypersonic Flight by Optimal Trajectory Control," AIAA Paper 1996-3905, 1996.

[13] Ardema, M. D., Bowles, J. V., and Whittaker, T., "Near-Optimal Propulsion-System Operation for an Air-Breathing Launch Vehicle," *Journal of Spacecraft and Rockets*, Vol. 14, No. 6, 1995, pp. 951–956.

[14] Ardema, M. D., Bowles, J. V., and Whittaker, T., "Optimal Trajectories for Hypersonic Launch Vehicles," *Dynamics and Control*, Vol. 4, No. 4, 1994, pp. 337–347.

[15] Ardema, M. D., Chou, H.-C., and Bowles, J. V., "Near-Optimal Operation of Dual-Fuel Launch Vehicles," *Journal of Guidance, Control, and Dynamics*, Vol. 19, No. 5, 1996, pp. 1180–1182.

[16] Chou, H.-C., Ardema, M. D., and Bowles, J. V., "Near-Optimal Re-Entry Trajectories for Reusable Launch Vehicles," AIAA Paper 1997-3582, 1997.

[17] Vukelich, S. R., Stoy, S. L., Burns, K. A., Castillo, J. A., and Moore, M. E., "Missile Datcom," Vol. 1, U.S. Air Force Flight Dynamics Lab., Rept. AFWAL-TR-86-3091, Wright–Patterson AFB, OH, 1988.

[18] Blake, W. B., "Missile Datcom: User's Manual—1997 Fortran 90 Revision," U.S. Air Force Research Lab., Rept. AFRL-VA-WP-TR-1998-3009, Wright–Patterson AFB, OH, 1998.

[19] Simon, J. M., and Blake, W. B., "Missile Datcom—High Angle of Attack Capabilities," AIAA Paper 99-4258, 1999.

[20] Hoak, D. E., "USAF Stability and Control Datcom," U.S. Air Force Flight Dynamics Lab., Rept. AFWAL-TR-83-3048, Wright–Patterson AFB, OH, 1960 (rev. 1978).

[21] Williams, J. E., and Vukelich, S. R., "The USAF Stability and Control Digital Datcom," Vol. 1, U.S. Air Force Flight Dynamics Lab., Rept. AFFDL-TR-79-3032, Wright–Patterson AFB, OH, 1979.

[22] Williams, J. E., and Vukelich, S. R., "The USAF Stability and Control Digital Datcom," Vol. 2, U.S. Air Force Flight Dynamics Lab., Rept. AFFDL-TR-79-3032, Wright–Patterson AFB, OH, 1979.

[23] Quinn, R. D., and Gong, L., "A Method for Calculating Transient Surface Temperatures and Surface Heating Rates for High-Speed

Aircraft," NASA TP-2000-209034, 2000.
[24] Gnoffo, P. A., and Inger, G. R., "Analytic Corrections to CFD Heating Predictions Accounting for Changes in Surface Catalysis, Part 2," AIAA Paper 96-4589, 1996.
[25] Quinn, R. D., and Gong, L., "Real-Time Aerodynamic Heating and Surface Temperature Calculations for Hyeprsonic Flight Simulation," NASA TM-4222, 1990.
[26] Quinn, R. D., and Palitz, M., "Comparison of Measured and Calculated Turbulent Heat Transfer on the X-15 Airplane at Angles of Attack up to 19.0°," NASA, TM X-1291, 1966.
[27] Fay, J. A., and Riddell, F. R., "Theory of Stagnation Point Heat Transfer in Dissociated Air," *Journal of the Aeronautical Sciences*, Vol. 25, No. 2, 1958, pp. 73–85,121.
[28] Beckwith, I. E., and Gallagher, J. J., "Local Heat Transfer and Recovery Temperatures on a Yawed Cylinder at a Mach Number of 4.15 and High Reynolds Numbers," NASA TR R-104, 1961.
[29] Moeckel, W. E., "Oblique-Shock Relations at Hypersonic Speeds for Air in Chemical Equilibrium," NACA TN-3895, 1957.
[30] Hansen, C. F., "Approximations for the Thermodynamic and Transport Properties of High-Temperature Air," NASA, TR R-50, 1959.
[31] Press, W. H., Teukolsky, S. A., Vetterling, W. T., and Flannery, B. P., "Integration of Ordinary Differential Equations," *Numerical Recipes in C: The Art of Scientific Computing*, 2nd ed., Cambridge Univ. Press, New York, 1992, pp. 707–752.
[32] Cowart, K., and Olds, J., "Integrating Aeroheating and TPS into Conceptual RLV Design," AIAA Paper 99-4806, 1999.
[33] Cowart, K., and Olds, J., "TCAT—A Tool for Automated Thermal Protection System Design," AIAA Paper 2000-5265, 2000.
[34] Blake, W. B., and Simon, J. M., "Tools for Rapid Analysis of Aircraft and Missile Aerodynamics," AIAA Paper 1998-2793, 1998.

J. Martin
Associate Editor